

# Neural Network Architectures for Optical Channel Nonlinear Compensation in Digital Subcarrier Multiplexing Systems

ALI BAKHSHALI\*, HOSSEIN NAJAFI, BEHNAM BEHINAEIN HANGINI,  
AND ZHUHONG ZHANG

Ottawa Optical Competency Center, Huawei Technologies Canada, 303 Terry Fox Dr, Kanata K2K 3J1  
\*ali.bakhshali@huawei.com

**Abstract:** In this work, we propose to use various artificial neural network (ANN) structures for modeling and compensation of intra- and inter-subcarrier fiber nonlinear interference in digital subcarrier multiplexing (DSCM) optical transmission systems. We perform nonlinear channel equalization by employing different ANN cores including convolutional neural networks (CNN) and long short-term memory (LSTM) layers. We start to compensate the fiber nonlinearity distortion in DSCM systems by a fully-connected network across all subcarriers. In subsequent steps, and borrowing from fiber nonlinearity analysis, we gradually upgrade the designs towards modular structures with better performance-complexity advantages. Our study shows that putting proper macro structures in design of ANN nonlinear equalizers in DSCM systems can be crucial for practical solutions in future generations of coherent optical transceivers.

## 1. Introduction

For high-speed long-haul fiber-optic transmission, the nonlinear interference from Kerr effect is a major bottleneck that limits the achievable transmission rates. This interference can be equalized by approximating and inverting the nonlinear Schrodinger equation through digital back-propagation (DBP) [1–3] or perturbation-based nonlinear compensation (PNLC) [4, 5]. However, large computational complexities and also the need for accurate data from the propagation link have limited their application in real-time processing with agile and flexible requirements.

Alternatively, a variety of ANN solutions have been recently proposed for fiber nonlinearity compensation application. The primitive works tried to squeeze additional performance by feeding triplets inspired from perturbation analysis of fiber nonlinearity to a feed-forward neural network [6]. Later works draw inspiration from DBP and aimed to incorporate deep convolutional neural networks (CNNs) for this tasks [7, 8]. The use of advance recurrent neural networks (RNNs), such as long short-term memory (LSTM) modules, which are more suitable for the equalization of time-series processes has also picked up a great interest [9, 10]. In fact, the pattern and medium dependent characteristics of nonlinear propagation make it a suitable problem to be tackled by variety of solutions from artificial neural network domain. In general, an ANN-based nonlinear equalizer is more flexible compared to the conventional methods in the sense that it can be better updated for different transmission scenarios without the need for accurate feedback of the channel parameters. Also, ANN nonlinear equalizers can be extended to include the functionalities of traditional DSP modules to create a more general equalizer. Furthermore, the ANN design where the compensation process is learned through data can potentially lead to a large reduction in computational complexity [11].

In this work, we consider an application of ANN in coherent optical communications. We focus on advanced ANN structures with the ability to generate appropriate features without any reliance on an external module for feature generation. We particularly study digital subcarrier multiplexing (DSCM) systems since their design flexibility makes it a promising solution for the coherent optical modems. Simplifying the DSP with lower speed processing per-subcarrier, flexible channel-matched transmission, robust clock recovery, and the easy transition to a

point-to-multi-point (P2MP) architecture are some of the advantages of DSCM systems.

Here, we develop *macro* ANN structures, inspired by the fiber nonlinearity distortion mechanism that governs the nonlinear interaction across different subcarriers that has shown to be more efficient in terms of inference complexity, model representation, and the ability to be trained. We propose various ANN structures for modeling and compensation of intra- and inter-subcarrier fiber nonlinearities in DSCM systems, and explore scalability and performance versus complexity tradeoffs of the presented solutions. Different models are designed in terms of how received symbols across digital subcarriers are employed for training ANN cores for intra-subcarrier self-phase modulation (iSPM) and inter-subcarrier cross-phase modulation (iXPM) nonlinear impairments. Starting with a fully-connected network across all subcarriers, we move toward upgrading the design with modular ANN cores and sequential training stages. In other words, we start with black-box ANN models and then propose more efficient and flexible modular designs inspired by nonlinear perturbation analysis. All models in here are universal from ANN-core choice perspective. Specifically, we choose the building block for all the proposed structures in this work to be an ANN core with combinations of CNN and LSTM layers. One important aspect in this work is to generalize the neural network designs such that a block of data is generated in the equalization since parallelization is an essential feature of the coherent modems. We explore parallelization of these designs and impact of block-processing on performance versus complexity tradeoffs for these models. We show that one can get orders of magnitude reduction in computational complexity by moving towards block equalization in this fashion.

The remainder of this paper is organized as follows: In Section 2, the base of nonlinear compensation for fiber channel is briefly discussed. In Section 3, the multi-purpose ANN-core structure as the building block of proposed models is explained. The details of various ANN structures for NLC in DSCM are presented Section 4 while Section 5 is devoted to the numerical setup and results comparison. Next, impact of dispersion map on the nonlinear equalizer designs is discussed in Section 6. Finally, we conclude the paper in Section 7.

## 2. Nonlinear Compensation for Optical Fiber Channel

The dual-polarization evolution of optical field over a fiber link can be explained by the Manakov equation [12] where the linear and nonlinear propagation impacts are described as follows:

$$\frac{\partial u_{x/y}}{\partial z} + \frac{\alpha}{2}u_{x/y} + j\frac{\beta}{2}\frac{\partial^2 u_{x/y}}{\partial t^2} = j\frac{8}{9}\gamma\left[|u_x|^2 + |u_y|^2\right]u_{x/y}, \quad (1)$$

where  $u_{x/y} = u_{x/y}(t, z)$  represents the optical field of polarization  $x$  and  $y$ , respectively,  $\alpha$  is the attenuation coefficient,  $\beta$  is the group velocity dispersion (GVD), and  $\gamma$  is the nonlinear coefficient. The nonlinear interference can be equalized by approximating and inverting the above equation through DBP [1–3] where the fiber is modeled as a series of linear and nonlinear sections through first-order approximation of Manakov equation. On the other hand, by employing the perturbation analysis [4], one can represent the optical field as the solution of linear propagation plus a perturbation term from the nonlinear impact in symbol domain and in one step for the accumulated nonlinearities. It is shown that the first-order perturbation term can be modeled by the weighted sum of triplets of transmitted symbols plus a constant phase rotation [5, 13].

A wide variety of machine learning solutions for fiber nonlinearity compensation in optical communications has been proposed in literature ([6–8, 10] among others). These solutions are generally benchmarked against conventional solutions such as DBP and PNLC. Considering the lumped nonlinear compensation methods, a block diagram for the equalization module is presented in Fig. 1 where the pre-processing buffer generates appropriate inputs for a given method. Specifically, it includes a module that calculates appropriate PNLC triplets for regular perturbation-based method or an artificial neural network nonlinear compensation (ANN-NLC) approach that operates on externally generated triplet features [6]. In ANN-NLC solutions that

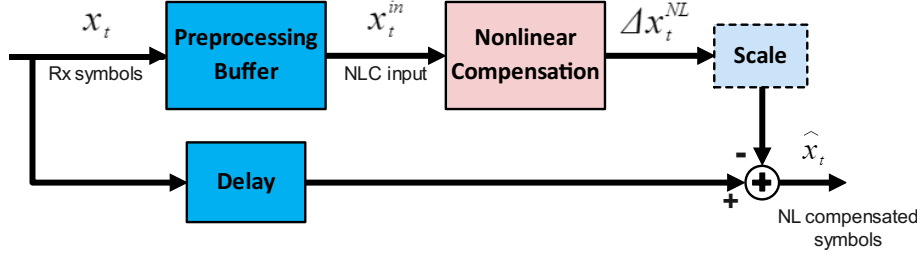


Fig. 1. Block diagram for lumped perturbation-based nonlinear compensation.

directly operate on Rx-DSP outputs [8, 10, 14, 15], this pre-processing buffer is tasked to provide an extended block of soft symbols needed to efficiently equalize the nonlinear interference.

Considering the first-order perturbation as the dominant nonlinear term, an appropriate scaling can be employed to adapt the nonlinear error estimates in case the training and inference stages are performed at different optical launch powers:

$$\alpha = 10^{(P_{\text{inference}}(\text{dB}) - P_{\text{train}}(\text{dB}))/10}. \quad (2)$$

where  $P_{\text{train}}$  is the optical launch power of the data used in the training while  $P_{\text{inference}}$  is the respective optical launch power of data in the inference (equalization) stage.

In this work, we consider various lumped ANN structures for modeling and compensation of fiber nonlinearity for DSCM systems. We provide the evolutionary approach of designing advanced ANN models that do not rely on external features (such as triplets) as input. Hence, by using symbols in a delay-line format as the input, the model learns relevant features according to its structures through additional layers. The proposed ANN-NLC equalizers estimate the nonlinear distortions of each subcarrier in one polarization of a DSCM signal given the relevant information from all digital subcarriers across both polarizations. Due to the nature of signal propagation in fiber and symmetries in the medium, it has been shown that the same model can be used to generate nonlinear error estimates for other polarization by simply swapping input signals to their respective counterpart from the first polarization. This alleviates the need to train separate models for X and Y polarization and enables efficient learning of a generalized model.

### 3. Multi-Purpose ANN-Core Structure

The presented ANN networks here mainly explore different higher level structures that aim to exploit the interaction between each target digital subcarrier and the neighboring ones in search for more powerful and efficient models. Hence, the models are universal from ANN-core choice perspective. Specifically, we choose the building block for all the proposed models in this work to be an ANN core comprising a combination of CNN and LSTM cores. In particular, we employ LSTM units that has been shown to have promising capability in efficient learning of complicated dynamic nonlinear systems. The first layer is a 1-dimensional CNN followed by Leaky ReLU activation function that is tasked with helping in feature generation. CNN features are fed into a LSTM module with bi-directional structure to extract time-dependency of the input features.

To save in computational resources for equalization, one can share the computational overhead corresponding to initialization of each LSTM chain by expanding the input and output sequences and provide estimates for multiple time instances. LSTMs are highly suitable to reduce the processing overhead of a sequential input stream since they aim to capture the most relevant representations of the past observed inputs in form of the hidden states. These hidden state variables are updated as new inputs are processed sequentially. However, the output remains an explicit function of the inputs and hidden state variables at every time instance. Consequently,

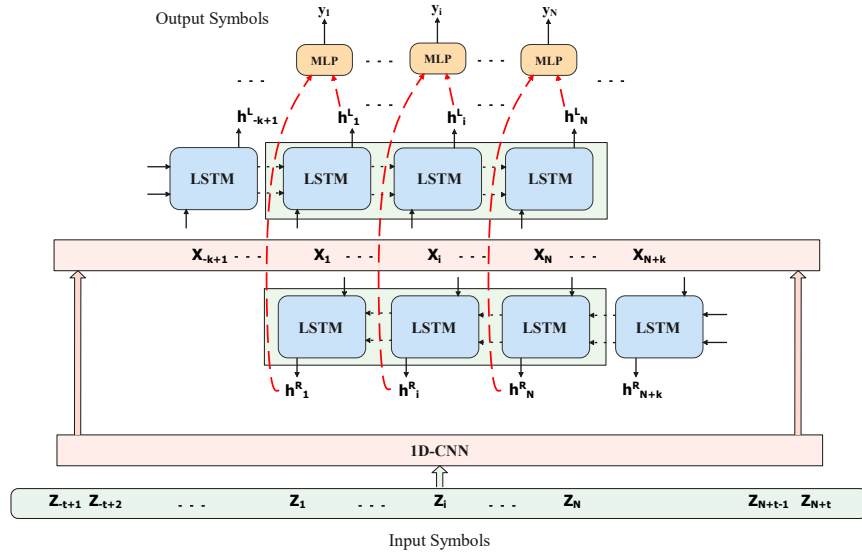


Fig. 2. Multi-purpose ANN-Core structure for the equalization path.

equalization of any extra input only increases the total computations by one extra RNN process step. To leverage this capability, simplify training, and to avoid the challenges from long back-propagation in LSTMs, these neural networks are trained with the regular symbol-based processing while the block-processing is employed during the deployment and evaluation stage. Note that by using the block-processing in equalization path, we bring an approximation into the network that we have trained with different initial hidden states. However, with long enough training block size and filter-tap in LSTM, one can show that the change in the states are minimal [15]. This is reflected in the complexity figures as we deploy trained models with different block sizes  $N$  in the numerical results.

A block diagram for the proposed ANN equalization core is depicted in Fig. 2. The LSTM network has been trained using a fixed sequence of features corresponding to  $2k + 1$  time instances, where  $k$  is the filter-tap size on each side of the target symbol. In the equalization path, we deploy the same network over input feature sequences corresponding to  $2k + N$  time instances to obtain output features associated to the symbols in the middle  $N$  time instances. In this case, input features corresponding to the first  $k + N$  time-instances  $i \in \{-k + 1, \dots, N\}$  are sequentially fed into a forward LSTM unit initialized with zero memory, producing output features and evolving the internal memory states. A similar, backward LSTM unit starts with zero memory and evolves using the CNN features corresponding to the last  $k + N$  time instances of the  $2k + N$  window  $i \in \{1, \dots, N + k\}$  in the opposite direction. Outputs of forward and backward LSTM modules for middle  $N$  time instances are concatenated to form the LSTM block outputs. Finally, the LSTM block outputs may pass through a linear or a multi-layer perceptrons (MLP) stage with Leaky ReLU activation functions (for all but the last layer) that ultimately provides estimations for real and imaginary part of nonlinear interference per output. Note that, as we discuss further in section 4, the final MLP layer can be separated from the ANN core and trained individually in some architectures.

In order to get a measure of complexity for the multi-purpose ANN core, we consider a CNN-LSTM network with an MLP output layer. Let us consider equalization of  $N$  symbols with processing window of  $N_w = 2t + N$ . The real multiplication per symbol (RM) for CNN is equal

to:

$$CNN_{RM} = \frac{4N_f N_{ke}(N_w - N_{ke} + 1)}{N}, \quad (3)$$

where  $N_f$  is the number of filter,  $N_{ke}$  is the kernel size for four input channels corresponding to in-phase and quadrature symbols for X and Y polarizations. In case information from multiple subcarriers are fed as input to the ANN core  $N_f$  should be scaled accordingly. The convolutional layer is assumed to have zero padding with single stride and dilation. For LSTM network, consider the input sequence length for each direction as  $N_s = k + N$  where  $k = t - (N_{ke} - 1)/2$  is the extra symbol length at each side of LSTM input. In this case, the combined RMs for forward and backward LSTM is given by:

$$LSTM_{RM} = \frac{2N_s N_h (4(N_f + N_h) + 3)}{N}, \quad (4)$$

where  $N_h$  is the hidden size. Finally, for an MLP with single hidden layer at the output of LSTM network, the RM is described by:

$$MLP_{RM} = n_m \cdot 2N_h + 2n_m. \quad (5)$$

where  $n_m$  is the hidden layer size. In case MLP contains more than one hidden layer, extra multiplications should be added, accordingly. Furthermore, in the absence of any hidden layer,  $MLP_{RM} = 4N_h$  where 4 is the multiplication of 2 directions of LSTM and 2 outputs in I and Q for each output symbol.

Note that to obtain complexity for each structure in Section 4, we need to calculate and accumulate the RMs associated to ANN cores in the equalization path for all subcarriers. Thus, we mainly use the number of real multiplications per super-symbol (RMpS) as the complexity metric for each realization of an architecture. Note that super-symbol denotes the combined output symbols for all digital subcarriers across one polarization at each time instance. While we limit the scope of this paper to a DSCM system with four sub-carriers, this metric enables us to further compare the results with other single carrier and DSCM transmission systems that operate on the similar baudrate and tailored for the same throughput in future studies.

## 4. ANN Structures for NLC in DSCM

### 4.1. Common-Core (CC)

First structure for joint NLC in DSCM is a fully-connected black-box approach that contains only one ANN core. This single ANN core is tasked to provide nonlinear distortion estimates for all subcarriers of one polarization using a window of received symbols from all subcarriers in both polarizations (as depicted in Fig. 3a). Note that employing CC model which lacks any enforced structure that separates the iSPM and iXPM nonlinear contributions could be seen as a double-edge sword. In one hand, this increases the number of training parameters compared to a specialized physics-informed ANN where a predetermined structure is enforced on the ANN architecture. On the other hand, by lack of adding any structure on the construct of the network, we may allow maximum entanglement of iSPM and iXPM features through different layers of the ANN core. This can potentially lead to higher efficiency by allowing the network to avoid duplicating terms that could be shared in the absence of a single and fully-connected structure. However, there is always the possibility that the ANN core structure may not be inherently powerful enough for the underlying nonlinear mechanism to learn all the appropriate features even by allowing higher complexity realizations. This could severely limit the performance, especially in the absence of adequate training data and defeat this purpose.

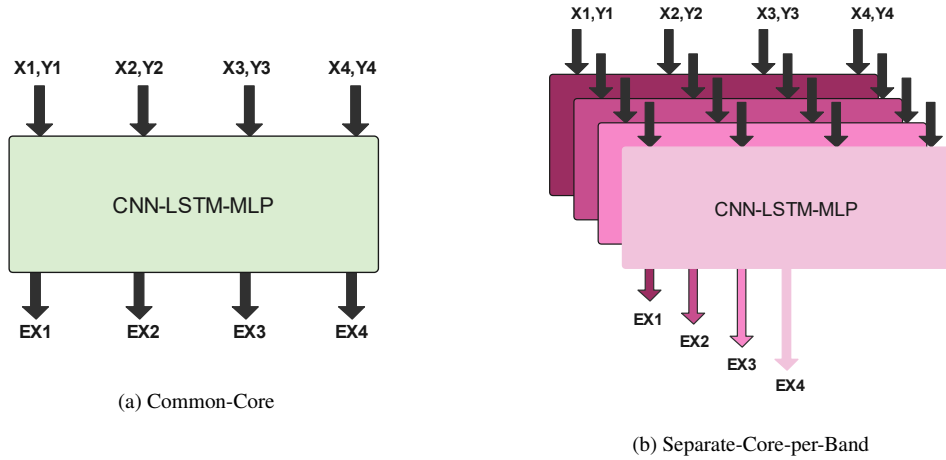


Fig. 3. ANN-NLC structures: (a) Common-Core, and (b) Separate-Core-per-Band

#### 4.2. *Separate-Core-per-Band (SC)*

In order to obtain a subcarrier-based structure and parallelize the model, we allocate a separate ANN core to estimate the nonlinear distortion for each subcarrier output. Note that similar to CC, ANN cores in SC still operate on input information from all subcarriers. This design is illustrated in Fig. 3b. The motivation here is to employ separate and smaller cores per subcarrier in order to be more effective in fine-tuning the model parameters. This is important since inner and outer subcarriers may experience different balances of iSPM and iXPM nonlinear distortions. Also, in terms of flexibility, in case there are inactive subcarriers due to the network throughput demands, such as hitless capacity upgrades or in P2MP scenarios, the parallel design in SC could be more efficiently deployed compared to the single connected core architecture of CC. However, one potential drawback for this structure is that utility sharing between equalization paths of different subcarriers is prevented.

#### 4.3. *Modular-1 (M1)*

We move on from the black-box approach to design more efficient and flexible ANN-NLC models by using the insights from perturbation analysis of fiber nonlinear propagation. Specifically, the underlying mathematics behind iSPM triplet coefficients in perturbation analysis weakly relies on the absolute position of a subcarrier in the spectrum [4]<sup>1</sup>. Also, iXPM nonlinearity mechanism relies on the relative position of target and interfering subcarriers. Hence, only a small set of iSPM and iXPM cores can be trained and multiple instances of these trained cores get deployed as needed in the equalization path. Furthermore, since iXPM contributions are more pronounced among neighboring subcarriers, smaller and more efficient networks can be deployed by involving only iXPM contributions of immediate neighboring subcarriers. Fig. 4a illustrates a set of ANN cores that can be trained for M1 design where one iSPM and four iXPM cores are trained to model the intra- and inter-subcarrier nonlinearities for up to two neighboring subcarriers from each side. Note that the input to an iSPM core is a window of the target subcarrier symbols while the iXPM cores employ symbols from both target and interfering subcarriers.

Let us look at an implementation of M1 model that considers iXPM nonlinearities of up to two neighboring interfering subcarriers from each side of every output subcarrier. The block diagram

<sup>1</sup>This statement is technically accurate in the absence of higher order linear distortion terms such as dispersion slope, but could be sufficiently accurate even in presence of such terms in practical systems.

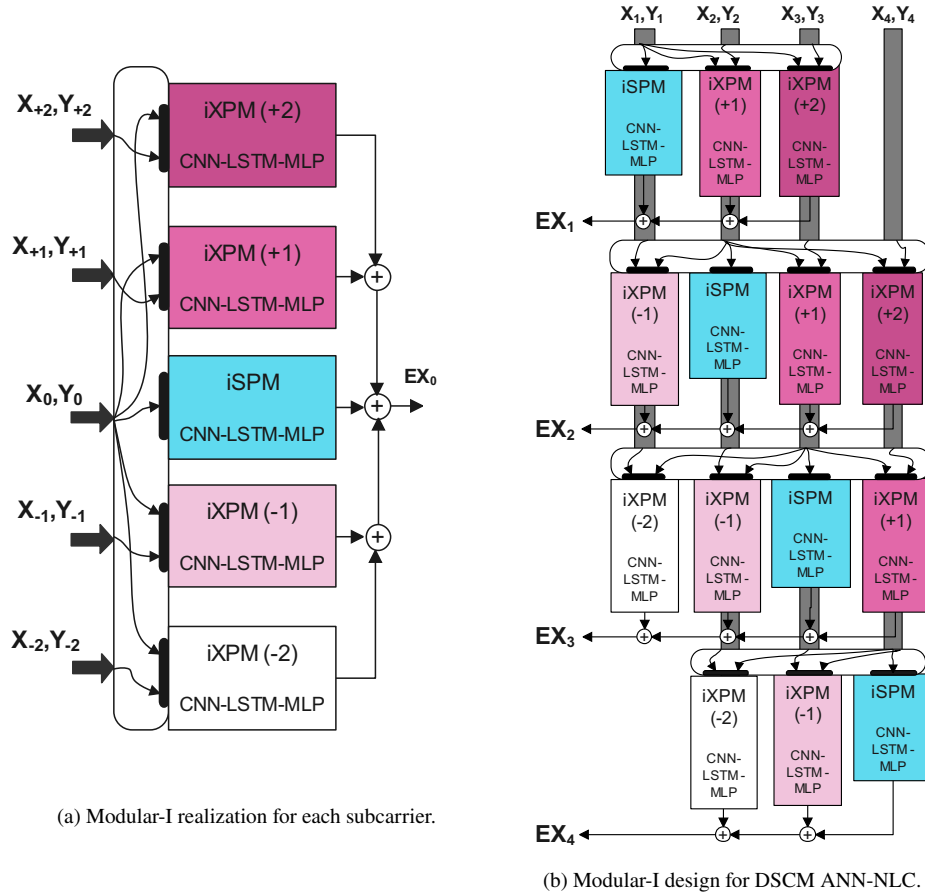


Fig. 4. Structural design of ANN-NLC using Modular-I. (a) illustrates the trained cores and (b) illustrates the implementation for a 4-subcarrier system.

for this modular NL equalizer is depicted in Fig. 4b where four iSPM cores compensate self nonlinearities originated from each subcarrier. Moreover, two inner and outer subcarrier pairs additionally employ three and two iXPM cores, respectively. Note that ANN cores with similar color share same layouts and weights leading to more efficient training specifically with limited data. Provided that channel parameters and subcarrier bandwidth and spacing remain the same, additional cores with learned weights and biases from this example can be deployed for systems with higher number of subcarriers. With a proper training strategy, the proposed structure allows us to separate iSPM and iXPM contributions and informatively direct computational resources to the best route. This is evident in the numerical results where we explore moving beyond iSPM compensation for various modular designs.

Another advantage of this modular design can be seen in certain scenarios, such as hitless capacity upgrades or in P2MP scenarios, wherein certain subcarriers could be turned-off. In this case, SC and specially CC models trained with all subcarriers may not be efficiently utilized as the statistics of inputs to ANN core(s) for the deactivated subcarrier(s) would be vastly different from the training. Additionally, it would be almost impossible to effectively identify and disable routes within ANN that correspond to the absent subcarriers to save power or reduce penalty. However, a modular design can be readily reconfigured to accommodate such scenarios

by deactivating the equalization paths corresponding to absent subcarriers, leading to a flexible and power-efficient deployment.

#### 4.4. Modular-II (M2)

The next step in the evolution of ANN-NLC for DSCM is rooted in two observations. First, the perturbation analysis [5, 13, 16] suggests that the iXPM perturbation coefficients  $C_{m,n}^{(-\ell)}$  governing the interaction of subcarrier  $i$  and its  $\ell$ 's neighbor on right  $i + \ell$  are similar to those of subcarrier  $i$  and its  $\ell$ 's neighbor on left  $i - \ell$ , provided that we employ a simple transformation, i.e.,

$$C_{m,n}^{(-\ell)} = C_{-m,n}^{(\ell)*} \quad (6)$$

where  $m$  and  $n$  are the symbol indices. Additionally, since these perturbation coefficients mainly rely on the relative position of subcarriers, the similarity can be extended to subcarrier  $i + \ell$  and its  $\ell$ 's neighbor on the left,  $i$ . Note that the iXPM(+ $\ell$ ) and iXPM(- $\ell$ ) cores in M1 for  $i$  and  $i + \ell$  subcarriers, respectively, are solely fed by inputs from these two subcarriers. This hints to potential computational savings by merging iXPM(+ $\ell$ ) and iXPM(- $\ell$ ) cores in M1 that operate on same subcarriers into a super core iXPM( $\pm\ell$ ) and potentially obtain a more efficient structure that preserve similar performance levels with a lower complexity.

The output features of these super-cores along with the appropriate iSPM features are passed to separate MLP modules prior to aggregation for each subcarrier. Note that MLP layers are detached from the ANN cores in this design and a set of  $2\ell + 1$  MLP modules are trained in this approach to model integration of iSPM features and up to  $2\ell$  iXPM core features involving neighboring subcarriers. The trained MLP modules are appropriately instantiated in the inference path for each subcarrier.

In summary, potential performance versus complexity tradeoff advantages of M2 could be of two fold. First, merging cores that are believed to contain significant amount of shared computations for feature generation can increase model efficiency. Second, reducing the distinct parameters of a network by replicating trained modules can greatly improve training efficiency and result in more generalized models. Also as mentioned before, the modular design provides

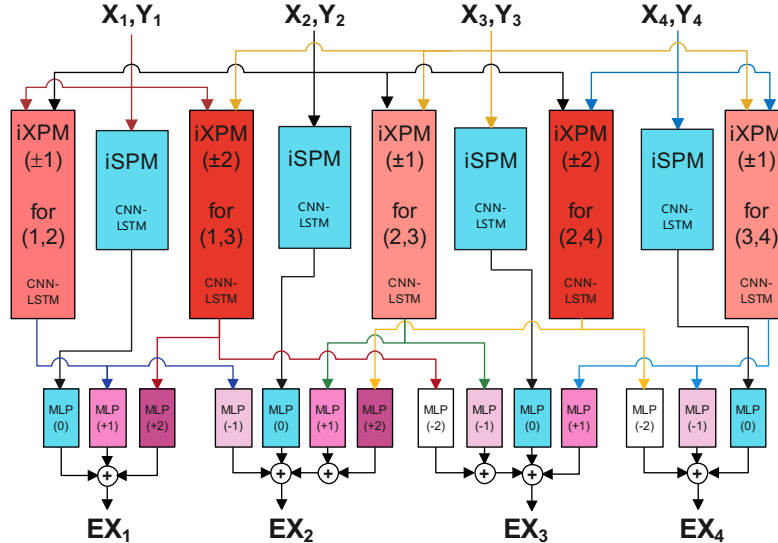


Fig. 5. Modular-II design for DSCM ANN-NLC.



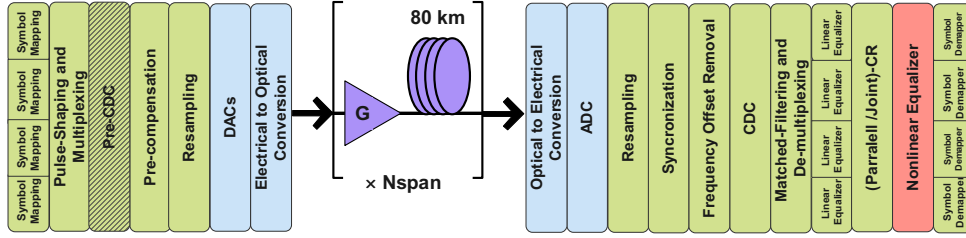


Fig. 6. System model for DSCM system.

additional flexibility in crafting more intelligent solutions for different network operational scenarios. Fig. 5 shows a block diagram for this model with four subcarriers and  $\ell = 2$ .

## 5. Numerical Results

### 5.1. System Model

The simulation setup includes typical Tx, channel, and Rx modules for a DSCM transmission scenario. To focus on fiber nonlinearity, we consider ideal electrical components and Mach-Zhender modulator. Also, DACs/ADCs are ideal with no quantization or clipping effects. The dual polarization fiber channel is modeled by split-step Fourier method [17] with adaptive step-size and maximum nonlinear phase-rotation of 0.05 degree to ensure sufficient accuracy. At the Rx side, the sequence output from carrier recovery (CR) are used to train and evaluate the nonlinear equalizer. Standard DSP algorithms are employed for detection and processing of the received signal at the Rx. The block diagram for such system is depicted in Fig. 6. Note that, to keep the ability of conventional coherent receiver for phase correction under correlated phase-noise (which is coming from nonlinear propagation in our case), we deployed the carrier recovery before ANN-NLC module. This ensures that the linear equalization provides nonlinear phase compensation capability of a coherent receiver without a dedicated NLC equalizer. Hence, the neural network compensation gain is given on top of the best linear performance.

To evaluate and optimize different algorithms, we focus on a single-channel DSCM system operating at 32 Gbaud with four subcarriers and uniform 16QAM modulation format. The signal at each subcarrier is digitally generated using root-raised cosine pulse shape with a roll-off factor of 1/16. The link consists of 40 spans of standard single-mode fiber of 80km length, followed by optical amplifiers with  $NF = 6$  dB noise figure. Furthermore, for the most of numerical results we consider a symmetric dispersion map, in which 50% of total dispersion is digitally pre-compensated at the transmitter side. This in turn allows us to simplify the diagrams and avoid unnecessary complications at this stage. Section 6 is devoted to extension of this design to other dispersion maps where we provide ANN-NLC structures optimized for a post-CDC scenario. The training and evaluation of models are performed using at 2 dBm launch power. This is close to the optimal launch power when DBP at 2 Sa/sym and 1 and 2 steps-per-span are employed to benchmark these results. Note that for this setup, a Q-factor of  $Q = 7.88$  dB can be obtained at the optimal launch power of 1 dBm in the absence of a fiber-nonlinearity compensation.

### 5.2. ANN Optimization Workflow

All the models here are trained and evaluated based on the simulation data using  $2^{18}$  symbols per digital subcarrier. The training and evaluation data are generated from pseudo-random streams and different generator seeds using permuted congruential generator (PCG64). Also, 20% of the training dataset was set aside for validation of the model during the training

Table 1. List of hyper-parameters for ANN core that operates on a sequence length  $T = 2t + 1$  with  $t \in [5 : 40]$ .

Layer	Learn-able Parameters	value / sweep range
CNN	<i>num_layers</i>	1
	<i>num_output_channels</i>	[10:200]
	<i>kernel_size</i>	[5:30]
LSTM	<i>num_hidden_state</i>	[10:300]
	<i>num_output_features</i>	[10:300]
MLP	<i>num_hidden_layers</i>	[0:2]
	<i>layer_size</i>	[10:100]

process. Root minimum squared error (RMSE) between the model outputs and the difference between transmitted symbols and the received values constitutes the loss, which is used in the back-propagation process to update the model coefficients. All models were trained using Adam optimizer with learning-rate = 0.001 for at least 200 epochs, unless terminated by the early-stopping mechanism that tracks the validation loss and prevents over-fitting. We mainly used mini-batches of length 512 in obtaining these results. Minor performance differences were observed by exploring mini-batch sizes as low as 128, and as high as 2048 provided that learning-rate and number of epochs were optimized accordingly. Additionally, we employed a learning-rate scheduler that reduces the learning-rate by 20% when loss stops reducing for 10 epochs. For each model, best coefficients associated to the least validation loss across all training epochs were saved at the end of the training stage.

In order to explore performance versus complexity tradeoff, more than a thousand models for each design are trained and tested in this work for different block-sizes. Table 1 illustrates the list of the ANN-Core hyper-parameters and their sweeping ranges. The sweeping resolution of each parameter within each participating ANN core are individually adjusted for each model structure. We use the scatter plots reflecting the performance-complexity of different realizations of each model based on a common test dataset obtained from a separate transmission simulation using noise and bit sequences of different random-number generator algorithms and seeds. The envelope associated to be best performing models at various complexity constraints are generated in order to compare different architectures.

### 5.3. Numerical Results Comparison

In this part, we provide performance versus complexity tradeoff comparison of various optimized ANN equalizers for different block-sizes. Fig. 7 illustrates the inference cost of various models in terms of RMpS. From ANN design point of view, it is important to efficiently allocate additional complexity in order to improve performance since majority of the models demonstrate subpar efficiency. As an example, increasing hidden size of LSTM may not be an efficient strategy to improve the performance if filter-tap size  $k$  is not large enough to capture the nonlinear memory.

It can be seen that using a separate ANN core per each subcarrier did not significantly change the outcome of SC compared to CC. Their best performance remains around 8.8 dB. The performance-complexity tradeoffs for these models remain very similar for different block sizes. One can clearly observe various advantages of modular solutions compared to the black-box approaches represented by CC and SC. Both modular solutions offer clear superiority in both low and high complexity regions while M2 structure, specifically, demonstrates superior performance complexity trade-off across all complexity regions among all structures. Note that the performance for iSPM compensation is capped around 8.6 dB. Employing additional cores to compensate for

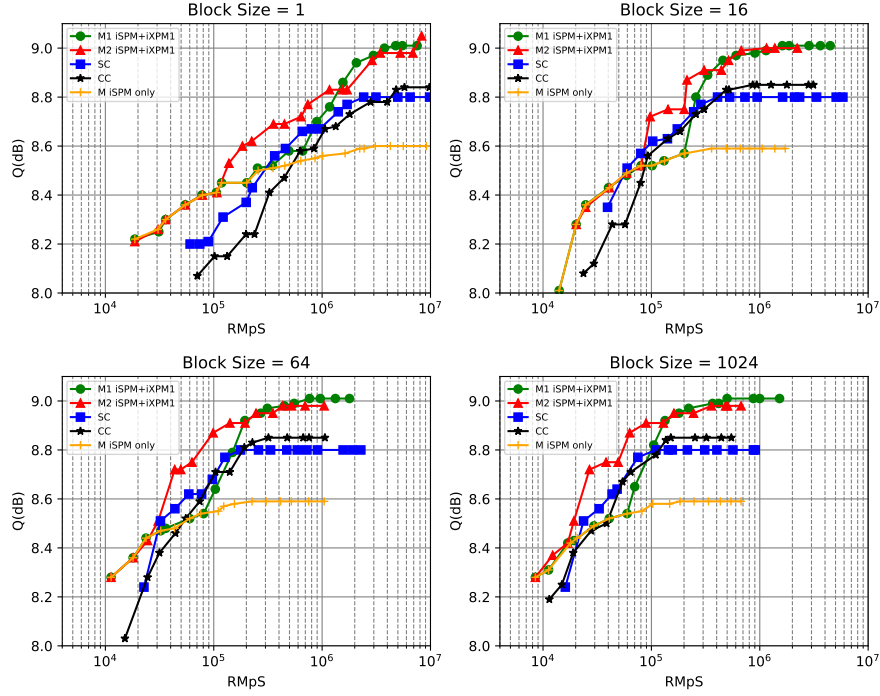


Fig. 7. A comparison of performance as a function of RMPs amongst different explored ANN-NLC solutions for DSCM.

intra-subcarrier nonlinearities due to immediate neighboring subcarriers  $\ell = 1$  from each side (iXPM1) can significantly increase the maximum performance to around 9 dB, unlocking 0.4 dB gain compared to the iSPM compensation at 2 dBm launch power. We further explored another scenario by incorporating iXPM contributions of two subcarriers from each side. However, the results are omitted as we did not observe a meaningful additional performance gain for this scenario. This result can be corroborated by findings in Section 6, where we demonstrate the perturbation coefficients corresponding to the iXPM contributions of the second neighbors for this setup showing that the magnitude of these coefficients are around 10dB lower than iXPM contributions from the immediate neighbors.

Note that the best performance obtained from modular solutions are generally 0.2 dB higher than CC and SC. This suggests that these solutions can more efficiently learn from a limited training data due to a more generalized structure with fewer trainable parameters. The trade-off between performance and complexity in mid-tier performance regions with Q around 8.6 dB is particularly noteworthy where non-modular designs can compete with M1. Note that this region is the onset of switching away from iSPM only NLC to incorporate iXPM nonlinearities from immediate neighboring subcarriers. This suggests that CC and SC architectures can converge to a moderately efficient structures by internally sharing resources of iXPM compensation between neighboring subcarriers. This type of resource sharing is one of the main distinctive features of M2 model compared to M1 that reflects in its superior efficiency in this region.

In order to demonstrate advantages of block-processing, performance versus complexity evaluations for different block-sizes are illustrated in Fig. 8 for M2 model as an example. A substantial complexity reduction for a very minimal performance loss can be obtained by parallelization of the trained ANN core and deploy the solution with a block-size  $N > 1$  provided that the model is sufficiently generalized in the training stage. In high-performance region

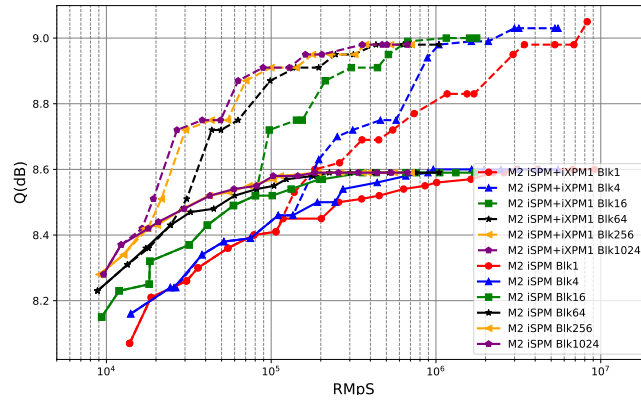


Fig. 8. Impact of block-size on performance vs. complexity of the best M2 models.

( $Q > 8.8$ ), we can achieve a complexity reduction by a factor of 20 for  $N = 1024$ . However, the complexity advantages shrinks in lower performance regions (ex. factor of 5 for  $Q \sim 8.4$ ) where best models generally have lower filter-tap size and incorporate less nonlinear memory.

Next, performance envelopes for all models as a function of the number of training parameters are depicted in Fig. 9. The number of training parameters is related to the memory requirements to store and retrieve model parameters as link configuration is modified over-time. This metric can also measure the efficiency of a model to provide a certain performance level with the least independent parameters which is also closely tied with generalization of the ANN. For a mid-tier performance of around 8.6 dB, the modular solutions generally demonstrate approximately 2 to 4 times lower number of parameters compared to CC and SC. Note that CC and SC solutions supposedly have access to all subcarrier information and are not limited to iSPM+iXPM1 architectures of M1 and M2. However, this assumed *advantage* results in a significant loss for CC and SC solutions if the number of training parameters are below 40,000. We attempted to close this performance gap by increasing the number of epoches for non-modular solutions and further optimizing the learning rates without much success. This may indicate that practical ANN design in presence of various limitations and constraints for this problem is far from a plug and play approach and requires careful design using insights from the physical model.

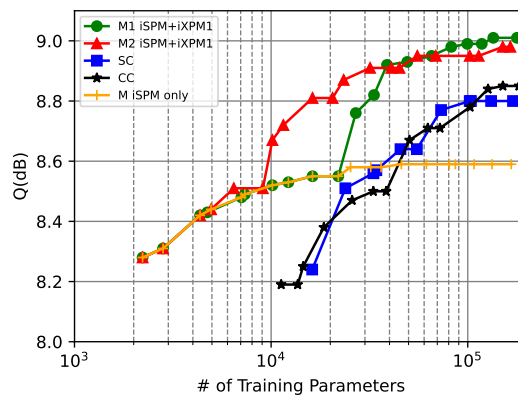


Fig. 9. A comparison of performance as a function of number of training parameters amongst different explored ANN-NLC solutions for DSCM.

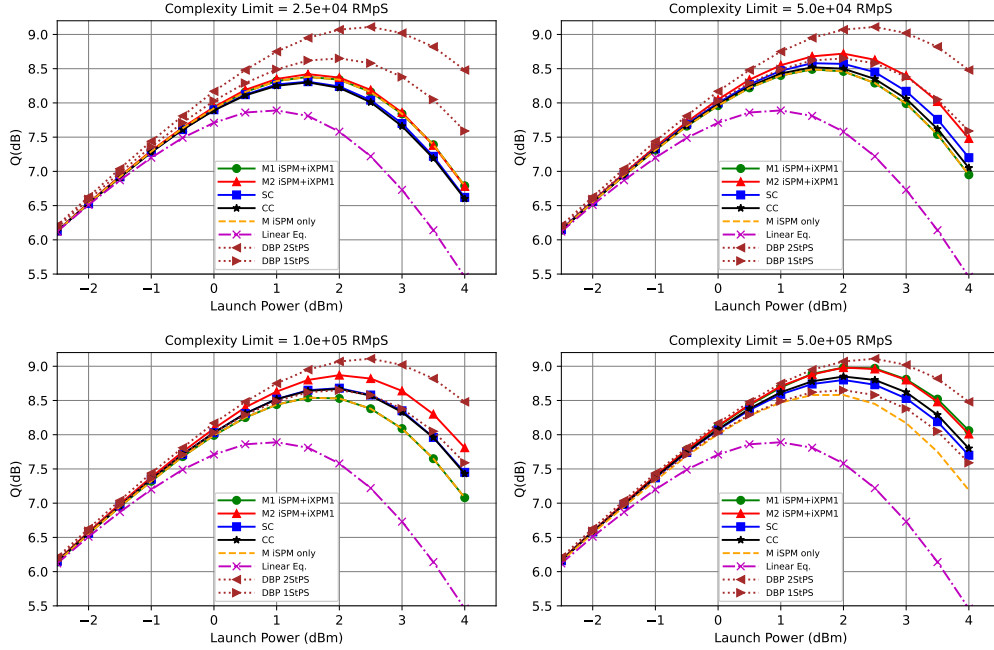


Fig. 10. Performance of different ANN-NLC solutions as a function of optical launch power for given complexity constraint budgets.

Finally, we explore the applicability of proposed models on similar links with different optical launch powers. Fig. 10 illustrates the performance as a function of optical launch power where multiple graphs are presented for best models obtained with different complexity budget constraints. As stated earlier, all models were trained at 2 dBm optical launch power. Note that selected models from all structures demonstrate good generalization and can provide nonlinear performance gain on a wide range of launch powers, spanning from linear regime to deep nonlinearity. We provide DBP performance plots with different number of steps per span (StPS) to benchmark proposed ANN-NLC structures. Note that, the complexity comparison with other NLC methods such as DBP is not performed here since a fair comparison requires development of efficient hardware-friendly versions of ANNs after model compression, pruning, and weight quantization which is beyond the scope of this paper.

## 6. Impact of Dispersion Map

So far, we have shown application of ANN-NLC equalizers in transmission scenarios with symmetric dispersion map. As depicted in Fig. 11, the windows for symbols of interest from target and interfering subcarriers for iSPM and iXPM triplet features for a symmetric dispersion map are symmetric around reference symbols. This is the main reason that symmetric windows of soft values are selected as input to iSPM and iXPM cores in the previous designs. However, in presence of an asymmetric dispersion map, such as post dispersion compensation, the regions for iXPM features of most significance are neither symmetric nor centered around the reference symbol from interfering subcarrier as shown in Fig. 12. Hence, one needs to adjust the input features for each iXPM core according to the dispersion-induced group-delay between the involved subcarriers. Another approach is to introduce delay lines in the input and output of the

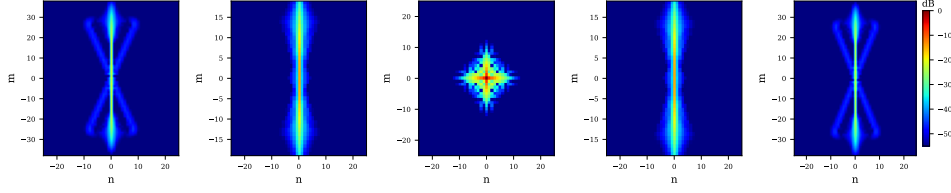


Fig. 11. Magnitude of iSPM ( $\ell = 0$ ) and iXPM ( $\ell \neq 0$ ) perturbation coefficients  $C_{m,n}^{(\ell)}$  for the DSCM simulation setup with sym-CDC: (a)  $\ell = -2$ , (b)  $\ell = -1$ , (c)  $\ell = 0$ , (d)  $\ell = 1$ , (e)  $\ell = 2$ .

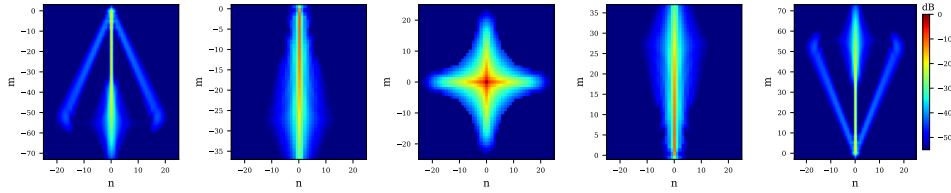


Fig. 12. Magnitude of iSPM ( $\ell = 0$ ) and iXPM ( $\ell \neq 0$ ) perturbation coefficients  $C_{m,n}^{(\ell)}$  for the DSCM simulation setup with post-CDC: (a)  $\ell = -2$ , (b)  $\ell = -1$ , (c)  $\ell = 0$ , (d)  $\ell = 1$ , (e)  $\ell = 2$ .

ANN equalizer and maintain a symmetric input windows for the ANN cores. Specifically, to ensure proper operation of the equalizer in this case, we introduce a progressive delay amounting to half of the dispersion-induced group delay between subcarriers prior to the ANN equalization. To reverse this impact, another delay-line is added at the out of the ANN equalizer. Note that the window size for each iXPM core needs to be as large as the maximum group-delay between associated subcarriers. This ensures symbols that impacted the target symbol are appropriately involved. Fig. 13 illustrates a block diagram for this solution.

We have modified the simulation setup to provide a performance comparison of selective ANN equalizers between symmetric- and post-CDC in Fig. 14. Similar trends are observed for CC and M2 solutions with post-CDC, showing the applicability and effectiveness of the proposed solution. Note that similar performance gains are achieved by switching from iSPM

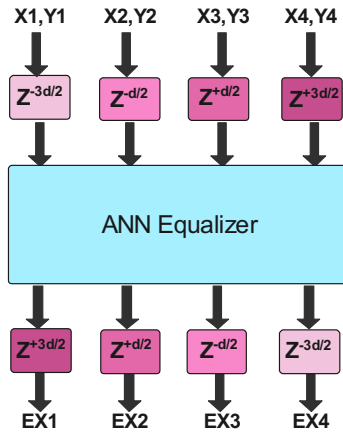


Fig. 13. Delay adjustment for post-CDC dispersion map.

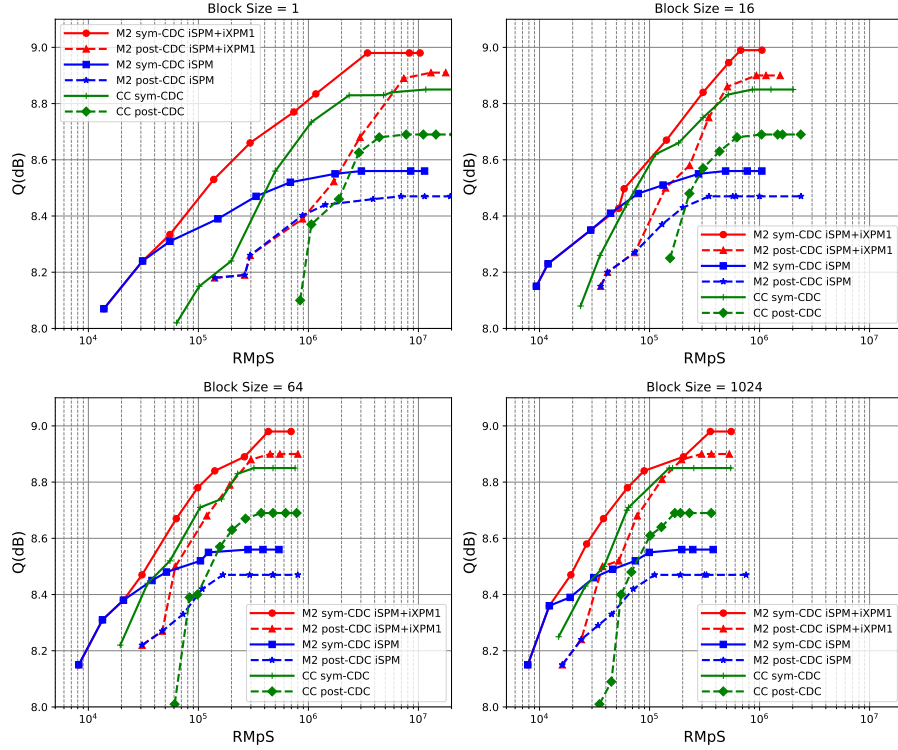


Fig. 14. Comparison on the impact of dispersion map on effectiveness of ANN-NLC using envelope associated to best performing models at different block-sizes.

to iSPM+iXPM1 nonlinear equalization for these schemes. Additionally, we observe that the complexity of all NLC solutions with post-CDC is higher than their respective counterpart with symmetric CDC for a given performance level. This can be attributed to the larger memory of iSPM and iXPM nonlinearities in the link with post-CDC. This is corroborated by comparing the domain and magnitude of perturbation coefficients presented in Fig. 11 and Fig. 12.

## 7. Conclusion

In this work, we studied different ANN approaches in compensation of intra-channel nonlinearities in DSCM systems. By training and evaluating various models over a comprehensive grid of parameters, we explored performance versus complexity tradeoff of each approach and discussed their scalability, potentials and weaknesses. Starting from back-box approaches in designing ANN models, we gradually moved towards modular designs inspired by perturbation analysis of fiber nonlinearity. This approach proved to be more efficient in training and producing better models with a given training data, as well as inference complexity and model storage requirements. We further demonstrate a pragmatic approach to adapt the proposed solutions to links with asymmetric dispersion maps. While these networks were exclusively designed for fiber nonlinearity compensation, a similar approach can be further studied in the context of component nonlinearity compensation in DSCM systems.

Note that all these designs can be further optimized by looking at other avenues. Notable approaches such as weight pruning, quantization and also future extension to quantization-aware training in form of quantized and binary neural networks can be explored to drastically reduce complexity of these models. Despite this, we believe that our presented study provides a fair

comparison and good starting step towards that path by focusing on the macro design of the ANN equalizers tailored to the characteristics of the fiber nonlinearity distortion mechanism in multi-subcarrier systems.

## References

1. E. Ip and J. M. Kahn, "Compensation of dispersion and nonlinear impairments using digital backpropagation," *J. Light. Technol.* **26**, 3416–3425 (2008).
2. L. B. Du and A. J. Lowery, "Improved single channel backpropagation for intra-channel fiber nonlinearity compensation in long-haul optical communication systems," *Opt. Express* **18**, 17075–17088 (2010).
3. E. F. Mateo, F. Yaman, and G. Li, "Efficient compensation of inter-channel nonlinear effects via digital backward propagation in WDM optical transmission," *Opt. Express* **18**, 15144–15154 (2010).
4. A. Mecozzi and R.-J. Essiambre, "Nonlinear Shannon limit in pseudolinear coherent systems," *J. Light. Technol.* **30**, 2011–2024 (2012).
5. Z. Tao, L. Dou, W. Yan, L. Li, T. Hoshida, and J. C. Rasmussen, "Multiplier-free intrachannel nonlinearity compensating algorithm operating at symbol rate," *J. Light. Technol.* **29**, 2570–2576 (2011).
6. S. Zhang, F. Yaman, K. Nakamura, T. Inoue, V. Kamalov, L. Jovanovski, V. Vusirikala, E. Mateo, Y. Inada, and T. Wang, "Field and lab experimental demonstration of nonlinear impairment compensation using neural networks," *Nat. Commun.* **10**, 1–8 (2019).
7. C. Häger and H. D. Pfister, "Nonlinear interference mitigation via deep neural networks," in *Optical Fiber Communication Conference*, (Optical Society of America, 2018), pp. W3A–4.
8. O. Sidelnikov, A. Redyuk, S. Sygletos, M. Fedoruk, and S. Turitsyn, "Advanced convolutional neural networks for nonlinearity mitigation in long-haul WDM transmission systems," *J. Light. Technol.* **39**, 2397–2406 (2021).
9. S. Deligiannidis, A. Bogris, C. Mesaritikakis, and Y. Kopsinis, "Compensation of fiber nonlinearities in digital coherent systems leveraging long short-term memory neural networks," *J. Light. Technol.* **38**, 5991–5999 (2020).
10. P. J. Freire, Y. Osadchuk, B. Spinnler, A. Napoli, W. Schairer, N. Costa, J. E. Prilepsky, and S. K. Turitsyn, "Performance versus complexity study of neural network equalizers in coherent optical systems," *J. Light. Technol.* **39**, 6085–6096 (2021).
11. I. Hubara, M. Courbariaux, D. Soudry, R. El-Yaniv, and Y. Bengio, "Quantized neural networks: Training neural networks with low precision weights and activations," *The J. Mach. Learn. Res.* **18**, 6869–6898 (2017).
12. P. K. A. Wai and C. Menyak, "Polarization mode dispersion, decorrelation, and diffusion in optical fibers with randomly varying birefringence," *J. Light. Technol.* **14**, 148–157 (1996).
13. Y. Gao, J. C. Cartledge, A. S. Karar, S. S.-H. Yam, M. O'Sullivan, C. Laperle, A. Borowiec, and K. Roberts, "Reducing the complexity of perturbation based nonlinearity pre-compensation using symmetric EDC and pulse shaping," *Opt. Express* **22**, 1209–1219 (2014).
14. P. J. Freire, A. Napoli, B. Spinnler, N. Costa, S. K. Turitsyn, and J. E. Prilepsky, "Neural networks-based equalizers for coherent optical transmission: Caveats and pitfalls," *IEEE J. Sel. Top. Quantum Electron.* **28**, 1–23 (2022).
15. H. Ming, X. Chen, X. Fang, L. Zhang, C. Li, and F. Zhang, "Ultralow complexity long short-term memory network for fiber nonlinearity mitigation in coherent optical communication systems," *J. Light. Technol.* **40**, 2427–2434 (2022).
16. F. Frey, L. Molle, R. Emmerich, C. Schubert, J. K. Fischer, and R. F. Fischer, "Single-step perturbation-based nonlinearity compensation of intra-and inter-subcarrier nonlinear interference," in *European Conference on Optical Communication (ECOC)*, (IEEE, 2017), p. P1.SC3.53.
17. G. P. Agrawal, "Nonlinear fiber optics," 2nd ed., New York: Acad. (1995).